

Supporting Information

**Electrochemically Synthesized Freestanding 3D Nanoporous Silver Electrode with High
Electrocatalytic Activity**

Lizhi Yuan,^{a,c} Luhua Jiang,^{*a} Tianran Zhang,^a Guoxiong Wang,^b Suli Wang,^a

Xinhe Bao,^b Gongquan Sun^{*a}

^a Dalian National Laboratory for Clean Energy, Dalian Institute of Chemical Physics, Chinese Academy of Sciences, Dalian 116023, China

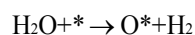
^b State Key Laboratory of Catalysis, Dalian Institute of Chemical Physics, Chinese Academy of Sciences, Dalian 116023, China

^c University of Chinese Academy of Sciences, Beijing 100039, China

E-mails: sunshine@dicp.ac.cn (L. Jiang), gqsun@dicp.ac.cn (G. Sun)

DFT calculation.

All the corresponding calculations were performed by the Vienna ab initio simulation package (VASP)¹ using periodic density functional theory (DFT). Projector augmented wave (PAW) method with generalized gradient approximation (GGA) of Perdew–Wang 1991 (PW91) was employed to describe valence-electron interactions.² The integration of the Brillouin zone was conducted using a $3 \times 3 \times 1$ Monkhorst–Pack grid. Energy cutoff was set at 400 eV and electron smearing was employed using Gaussian smearing technique with a width of 0.2 eV. Spin polarization calculation was carried out for all possible structures with the bottom two layers of the surface being fixed. Electronic energies were computed with the SCF tolerance of 10^{-5} eV and total forces were converged to less than 0.02 eV/Å. The binding energy of O (ΔE_{O}) and OH (ΔE_{OH}) was calculated according to the follow equations, respectively³:

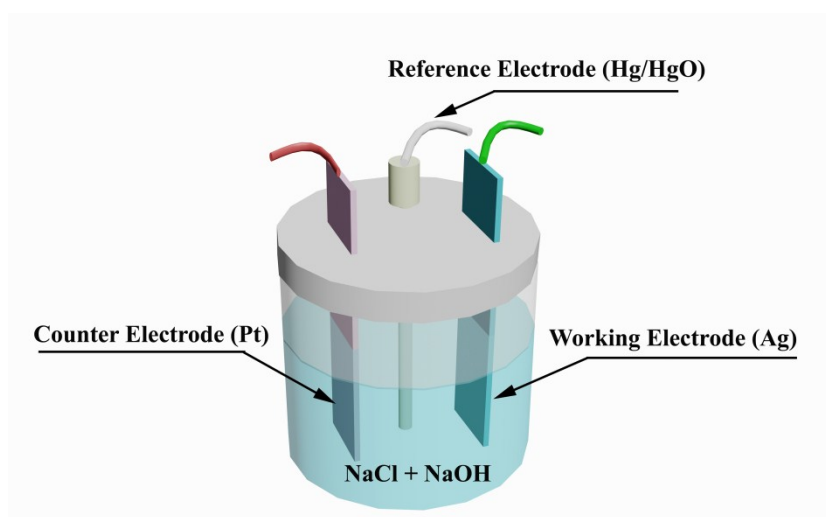


Where * is refer to the surface. The more positive of the binding energy, the weaker of the interaction between O or OH and surface.

The free-energy diagram was calculated referring to computed standard hydrogen electrode model (CSHE) reported by Nørskov et al..^{3,4} The free energy changes were then calculated as the difference between the products and reactants in each step, as shown below:

$$\Delta G(U, pH, T) = \Delta G_0 + \Delta G_U + \Delta G_{pH}$$

where $\Delta G_0 = \Delta E - \Delta \text{ZPE} + T\Delta S$, ΔE is the calculated total energy of the reaction, ZPE is the zero-point energy, S is the entropy, T is the temperature, ΔG_U and ΔG_{pH} is the correlation of potential and pH value.



At 1.2V:

WE (Anodic oxidation): $\text{Ag} + \text{Cl}^- \rightarrow \text{AgCl} + \text{e}^-$, CE (Cathodic reduction): $\text{H}_2\text{O} + \text{e}^- \rightarrow \text{OH}^- + 1/2 \text{H}_2$

At 0.12V:

WE (Cathodic reduction): $\text{AgCl} + \text{e}^- \rightarrow \text{Ag} + \text{Cl}^-$, CE (Anodic oxidation): $\text{Cl}^- \rightarrow 1/2 \text{Cl}_2 + \text{e}^-$

Scheme S1 Schematic illustration of the three-electrode cell setup used for preparation of np-Ag.

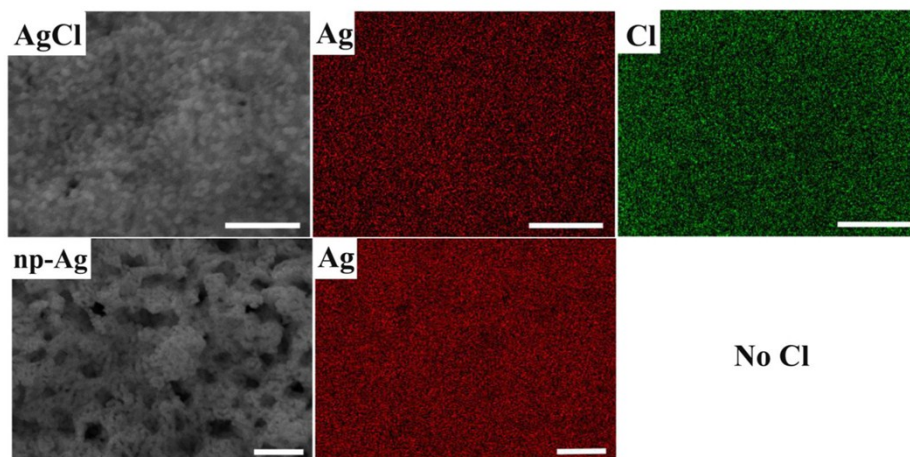


Fig. S1 SEM image of AgCl and the corresponding elemental mapping of Ag and Cl. SEM image of np-Ag and the corresponding elemental mapping of Ag.

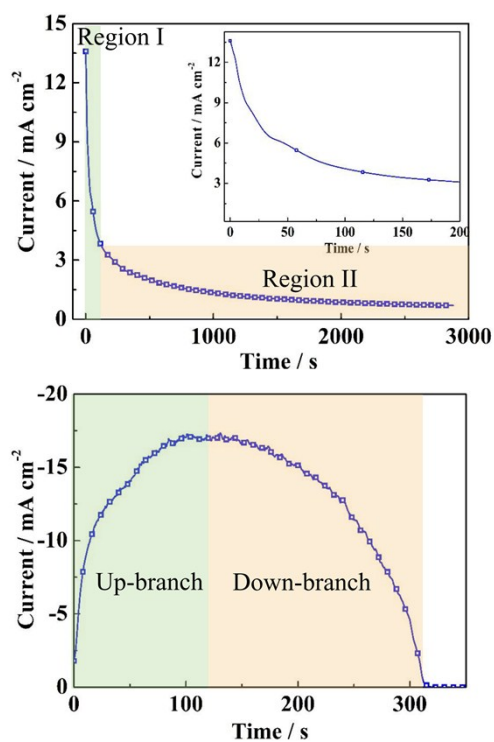


Fig. S2 (a) Potentiostatic curve for Ag electrode at 1.2 V in 0.1 M NaCl + 0.1 M NaOH electrolyte, The insert is the enlarged curve of (a) in the beginning 200 s, (b) Potentiostatic curve for AgCl-covered-Ag electrode at a potential of 0.82 V.

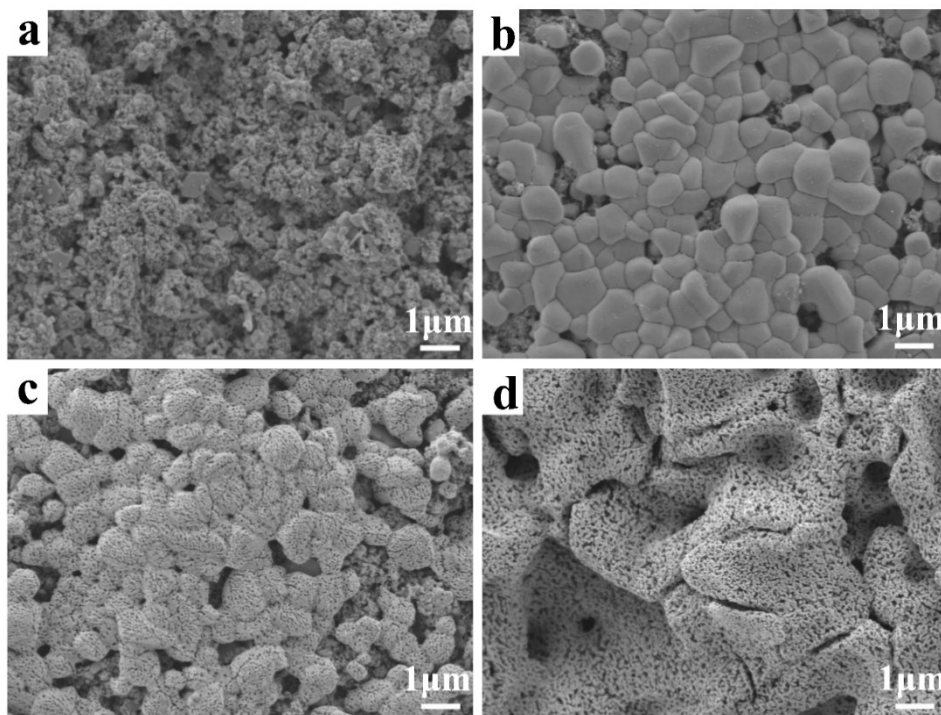


Fig. S3 (a) SEM image of Ag powder adhered to carbon diffusion layer, SEM images of AgCl obtained by oxidizing powdery Ag at 1.2 V for 2880 s (b) and np-Ag obtained by reducing AgCl at 0.12 V for 100 s (c), SEM image of np-Ag derived from Ag wire (0.2 mm in diameter) (d).

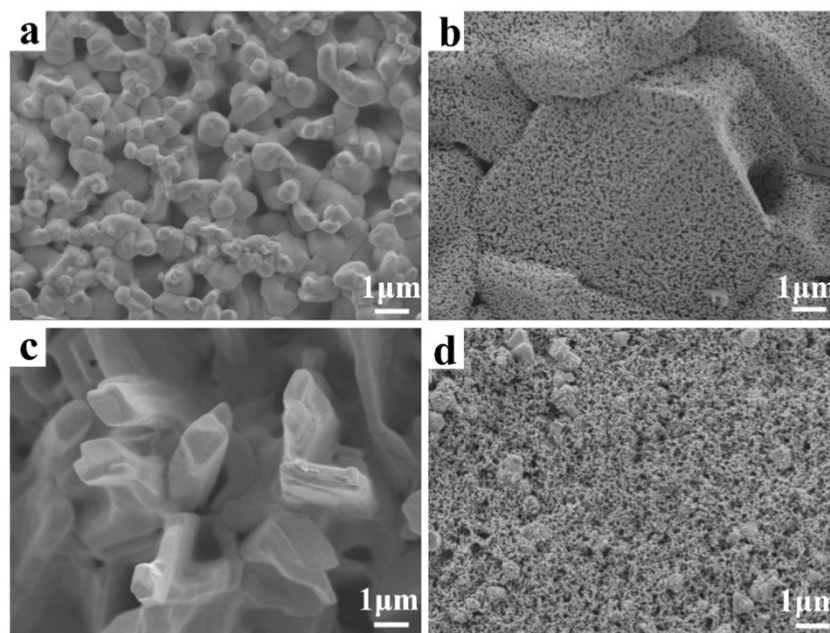


Fig. S4 SEM images of AgBr obtained from Ag sheet (a) and the corresponding np-Ag derived from AgBr (b), SEM images of AgI obtained from Ag sheet (c) and np-Ag derived from AgI (d).

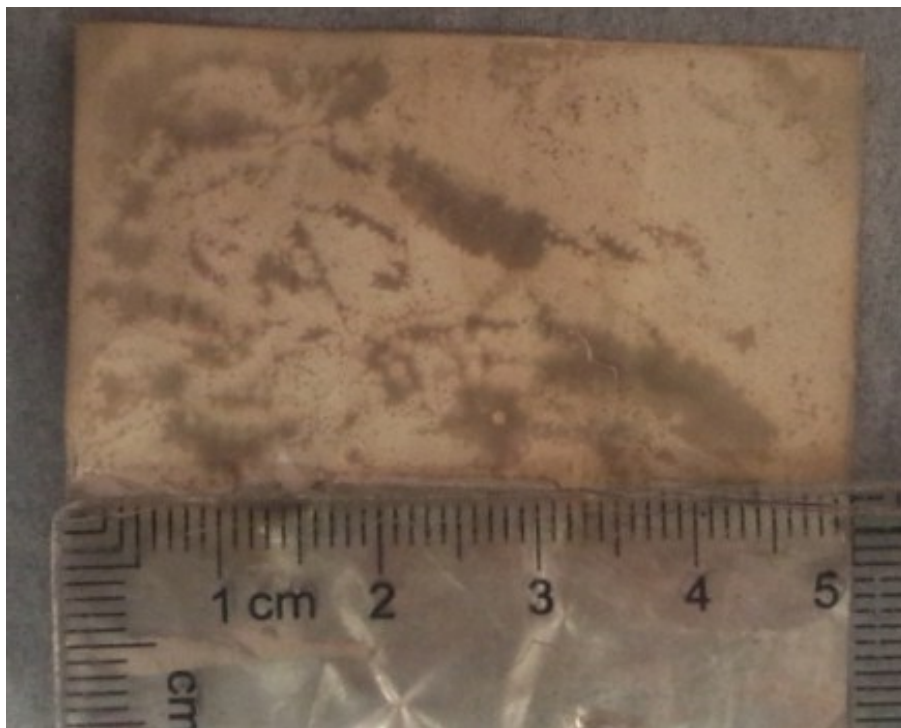


Fig. S5 Photograph of np-Ag obtained from Ag sheet.

The np-Ag was synthesized as follows. The pc-Ag sheet was oxidized at a constant potential of 1.2V in an electrolyte solution containing 0.1 M NaCl for 2880s. Then, the oxidized Ag sheet was kept at a potential of 0.12V for long enough time to allow the AgCl completely reduced to np-Ag. The obtained np-Ag was washed with DI water for several times and ready for use.

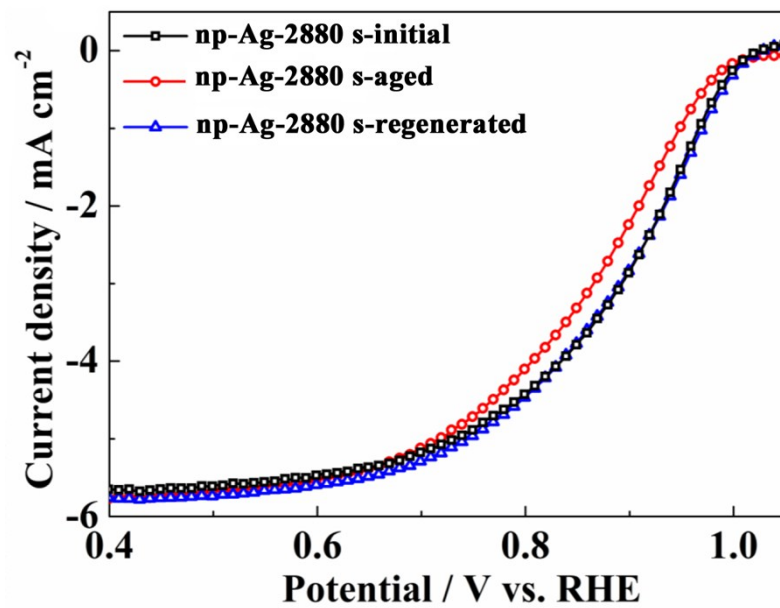


Fig. S6 ORR polarization curves measured in oxygen-saturated 0.1 M NaOH electrolyte. (rotation rate: 1600 rpm, scan rate: 10 mV s⁻¹).

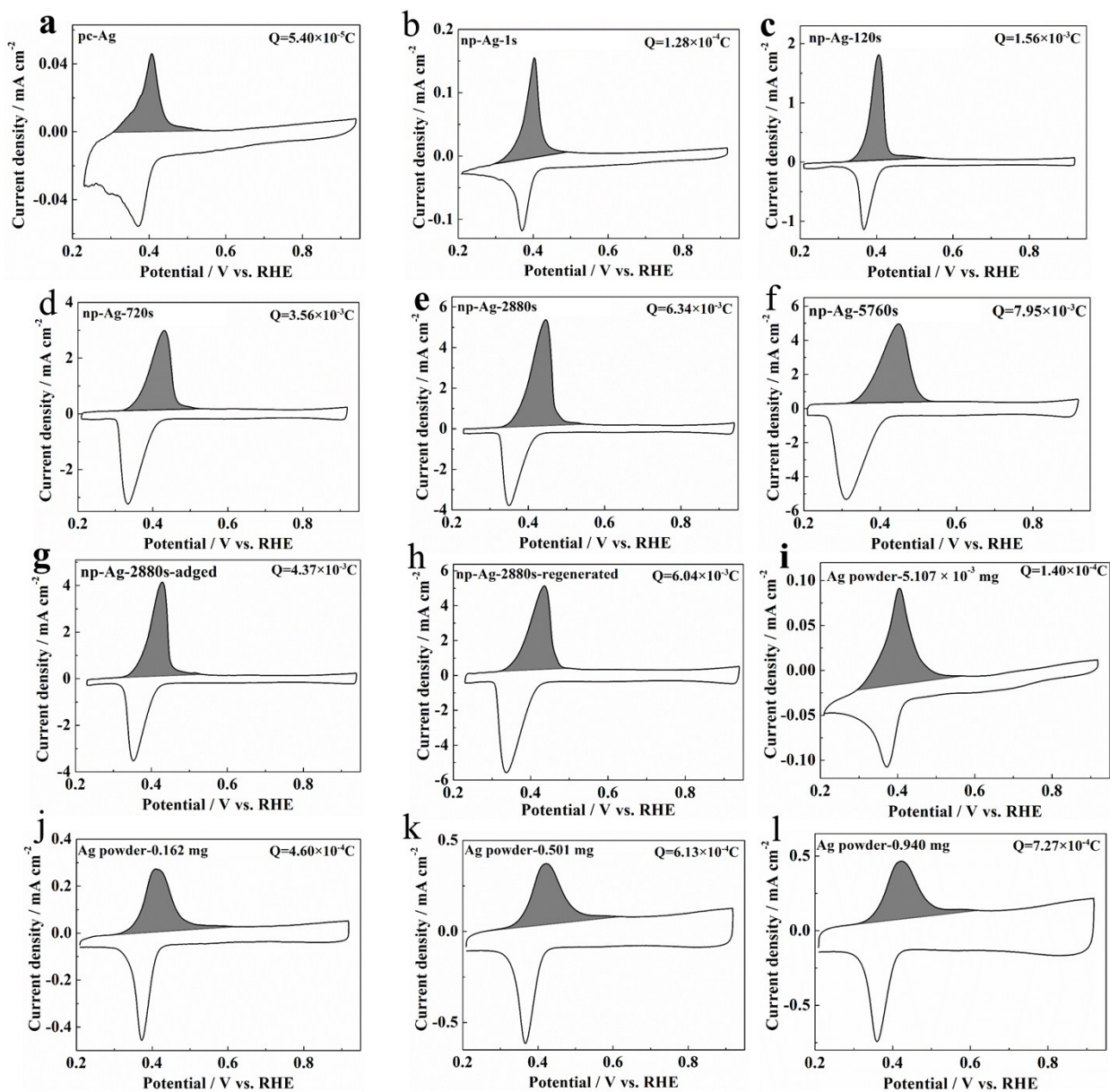


Fig. S7 Pb_{UPD} CV for the pc-Ag, np-Ag and Ag powder electrocatalyst.

Electrochemical surface area (ECSA) of silver is determined by Pb under potential deposition (Pb_{UPD}) using the theoretical value of 0.26 mC cm^{-2} for a monolayer of Pb on Ag surface and were listed in table S2^{1,2}.

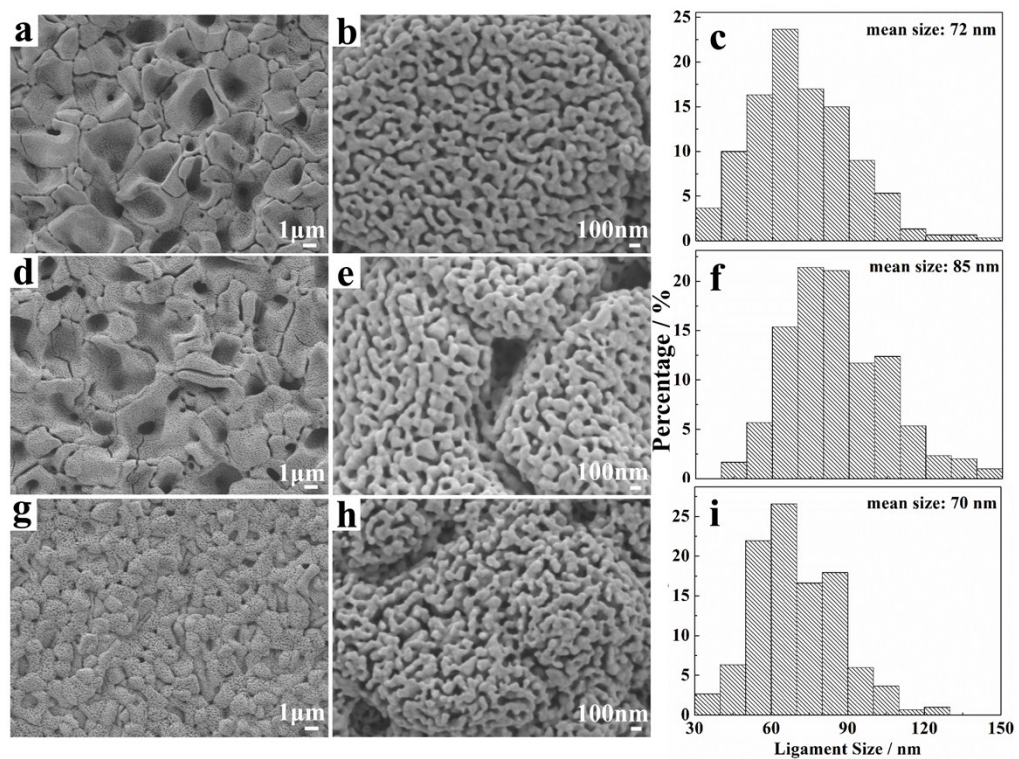


Fig. S8 SEM images of the initial (a-b), aged (d-e), and regenerated (g-h) np-Ag-2880s, the size histograms of the Ag ligament of the initial (c), aged (f), and regenerated (i) np-Ag-2880s.

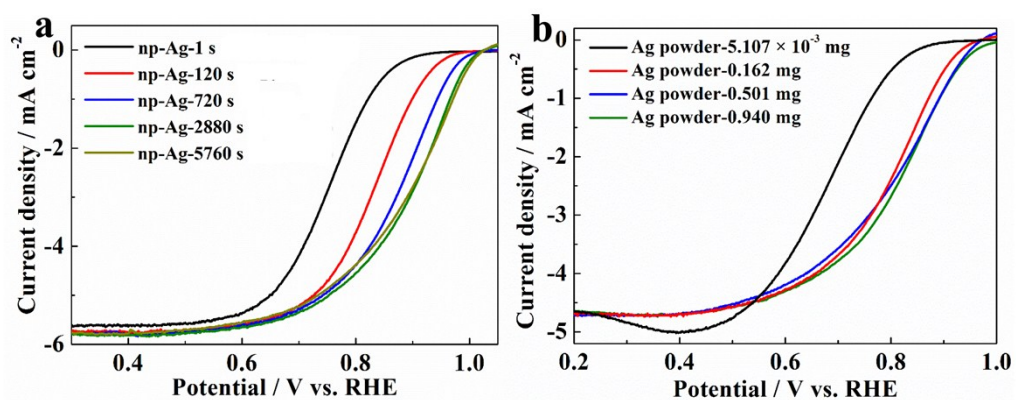


Fig. S9 ORR polarization curves of np-Ag and Ag powder electrode measured in oxygen-saturated 0.1 M NaOH electrolyte (rotation rate: 1600 rpm, scan rate: 10 mV s^{-1}). The np-Ag electrocatalysts were synthesized at the oxidation potential of 1.2 V with different times in 0.1 M NaCl and 0.1 M NaOH electrolyte, the Ag powder electrode were of the same mass to the np-Ag obtained with different oxidation times. The mass of the np-Ag were acquired by calculate the charge used during the np-Ag synthesise process (oxidation process or reduction process).

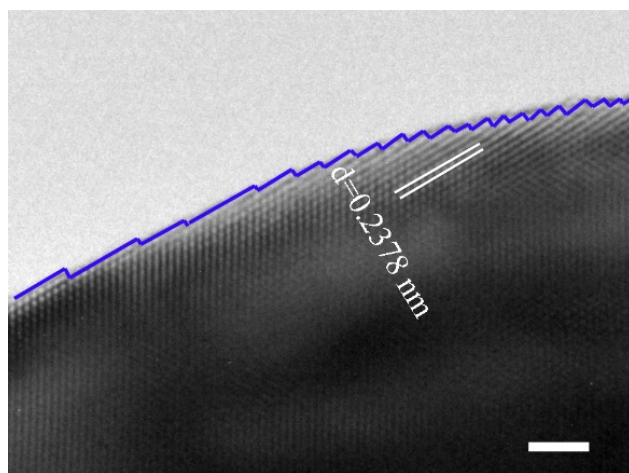


Fig. S10 The HRTEM image of the np-Ag

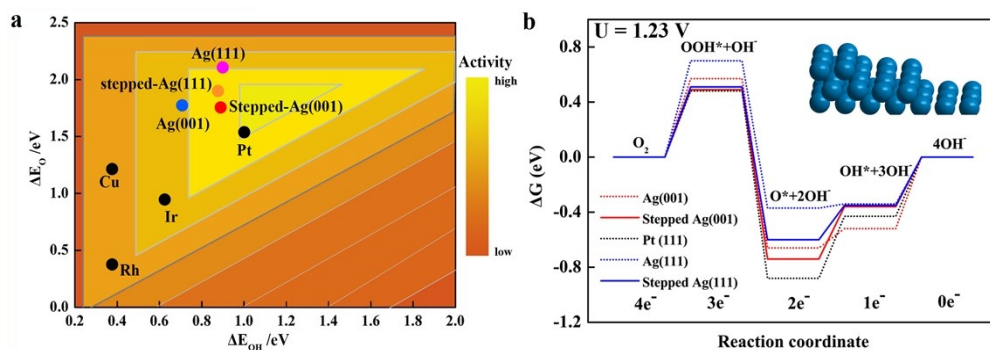


Fig. S11 (a) Oxygen reduction activity of stepped Ag(001) and stepped Ag(111) surfaces as a function of both the O and the OH binding energy, compared with perfect Ag(001) perfect Ag(111), Pt(111) surface and (111) surfaces of other metals. The trend and the activity of Cu, Ir, Ru are referred to the results of reference.³ **(b)** Calculated free energy diagrams for ORR on a stepped Ag(001) (red line), stepped Ag(111) (blue line), perfect Ag(001) (red dot line) and perfect Ag(111) (blue dot line) surfaces, compared to that of Pt(111) (black dot line). The inset shows the optimized structure of stepped Ag surface.

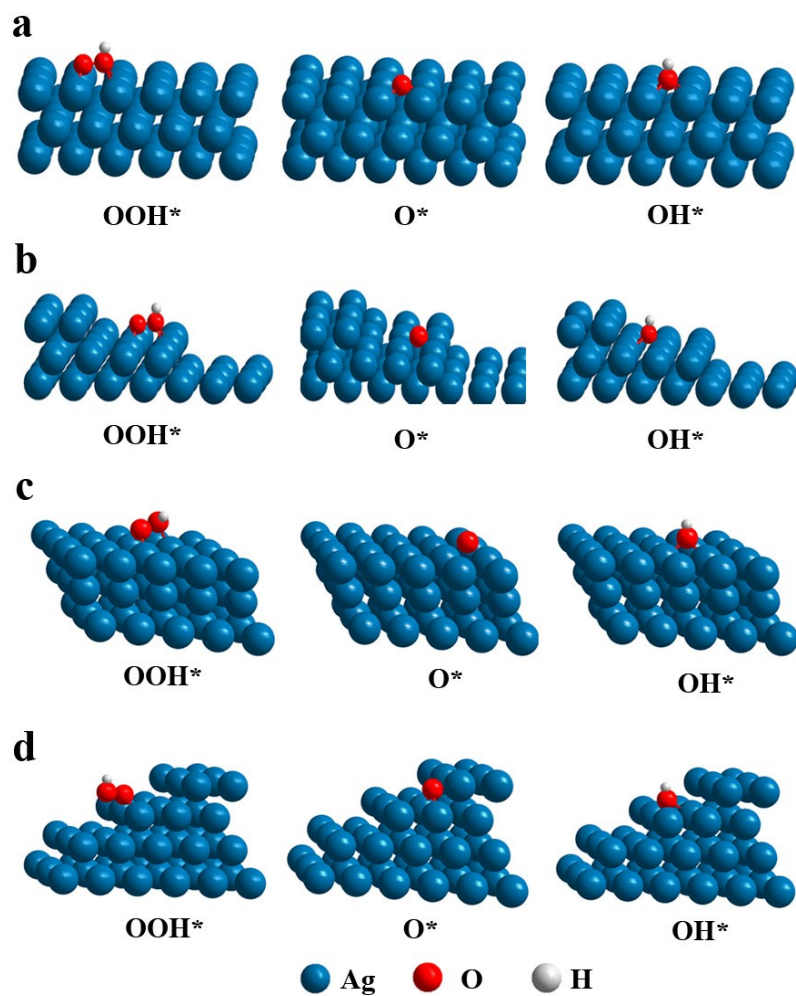


Fig. S12 Optimized adsorption structures of intermediates during the ORR modelling on perfect Ag(001) surface (a), stepped Ag(001) surface (b), perfect Ag(111) surface (c) and stepped Ag(111) surface (d).

Table S1 The half-wave potential, ECSA and thickness of catalysts.

Sample	$E_{1/2}$ (V)	ECSA ^a (cm ²)	Thickness (μm)	Ag mass ^b (mg)
pc-Ag	0.668	0.208	-	
np-Ag-1s	0.753	0.490	-	5.107×10^{-3}
np-Ag-120s	0.831	3.564	3.2	0.162
np-Ag-720s	0.874	13.692	9.5	0.501
np-Ag-2880s	0.900	24.385	14.5	0.940
np-Ag-5760s	0.897	30.562	32.5	1.242
np-Ag-2880s-aded	0.879	16.808	14.5	0.940
np-Ag-2880s-regenerated	0.899	23.231	14.5	0.940
Ag powder- 5.107×10^{-3} mg	0.688	0.538	-	5.107×10^{-3}
Ag powder-0.162 mg	0.803	1.769	-	0.162
Ag powder-0.501 mg	0.811	2.358	-	0.501
Ag powder-0.940 mg	0.818	2.796	-	0.940
Pt powder-0.940 mg	0.877	-	-	0.940

^a Electrochemical surface area (ECSA) of silver were determined by Pb under potential deposition (Pb_{UPD}) charges by assuming a factor of 0.26 mC cm^{-2} for a monolayer of Pb on Ag surface^{5, 6} according to the Pb_{UPD} curves shown in Fig. S7.

^b The Ag mass of the np-Ag catalysts were calculated by the following equation:

$$\text{Mass}_{\text{Ag}} = Q/F \times M_{\text{Ag}}$$

Q was obtained by integrating the charge of the cathodic current ($\text{AgCl} + e^- \rightarrow \text{Ag} + \text{Cl}^-$) during the np-Ag synthesis process; F is the Faraday constant (96485 C mol^{-1}); M_{Ag} is the molar mass of Ag (107.9 g mol^{-1}).

Table S2 Summary of half-wave potential ($E_{1/2}$) of the ORR over the Ag catalysts in literature.

Electrocatalysts	$E_{1/2}$ / V	Electrolyte	Rotating speed / rpm	Reference electrode	Ref.
np-Ag-2880 s	0.900	0.1 M NaOH	1600	RHE	This work
Ag powder-0.940 mg	0.818	0.1 M NaOH	1600	RHE	This work
pc-Ag	0.668	0.1 M NaOH	1600	RHE	This work
Pt black	0.876	0.1 M NaOH	1600	RHE	This work
AgNW 25 nm	0.797	0.1 M KOH	1600	RHE	[7]
np-Ag	0.860	0.1 M KOH	1600	RHE	[8]
AgCo	0.806	0.1 M NaOH	900	RHE	[9]
Ag	0.741	0.1 M NaOH	900	RHE	[9]
Ag(111)	0.643	0.1 M KOH	1600	RHE	[10]
Ag(100)	0.612	0.1 M KOH	1600	RHE	[10]
Ag(110)	0.697	0.1 M KOH	1600	RHE	[10]
Ag NWs	0.778	0.1 M KOH	1600	RHE	[11]
Ag/GO/C	0.700	0.1 M NaOH	1600	RHE	[12]
Ag ₄ Sn/C	0.682	0.1M KOH	1600	RHE	[13]
np-Ag-2880 s	-0.019	0.1 M NaOH	1600	MMO	This work
Ag/Mn ₃ O ₄ /C	-0.111	0.1 M NaOH	1600	MMO	[14]
Ag-Mo-22	-0.175	1 M KOH	1600	MMO	[15]
Ag ₄ Pd	-0.032	0.1 M KOH	1600	MMO	[16]
Ag/C	-0.162	1 M KOH	1600	MMO	[17]
Ag/Co ₃ O ₄ -C	-0.125	1 M KOH	1600	MMO	[17]
60% Ag/C	-0.174	1 M KOH	1600	MMO	[18]
Ag/C	-0.294	0.1 M NaOH	1600	MMO	[19]
Ag/RGO	-0.231	0.1 M NaOH	1600	MMO	[19]
Ag-MnO _x /C-300	-0.110	0.1 M NaOH	1600	MMO	[20]
MnPc@Ag/C	0.707	0.1 M NaOH	2500	RHE	[21]
FePc@Ag/C	0.851	0.1 M NaOH	2500	RHE	[21]
CoPc@Ag/C	0.743	0.1 M NaOH	2500	RHE	[21]
NiPc@Ag/C	0.701	0.1 M NaOH	2500	RHE	[21]

Supplementary References:

1. G. Kresse and J. Furthmüller, *Phys. Rev. B*, 1996, **54**, 11169-11186.
2. P. E. Blöchl, *Phys. Rev. B*, 1994, **50**, 17953-17979.
3. J. K. Nørskov, J. Rossmeisl, A. Logadottir, L. Lindqvist, J. R. Kitchin, T. Bligaard and H. Jónsson, *J. Phys. Chem. B*, 2004, **108**, 17886-17892.
4. G. S. Karlberg, J. Rossmeisl and J. K. Nørskov, *Phys Chem Chem Phys*, 2007, **9**, 5158-5161.
5. G. Wiberg, K. Mayhofer and M. Arenz, *ECS Transactions*, 2009, **19**, 37-46.
6. G. K. H. Wiberg, K. J. J. Mayrhofer and M. Arenz, *Fuel Cells*, 2010, **10**, 575-581.
7. S. M. Alia, K. Duong, T. Liu, K. Jensen and Y. Yan, *ChemSusChem*, 2012, **5**, 1619-1624.
8. Y. Zhou, Q. Lu, Z. Zhuang, G. S. Hutchings, S. Kattel, Y. Yan, J. G. Chen, J. Q. Xiao and F. Jiao, *Adv. Energy. Mater.*, 2015, DOI: 10.1002/aenm.201500149, n/a-n/a.
9. A. Holewinski, J.-C. Idrobo and S. Linic, *Nat. Chem.*, 2014, **6**, 828-834.
10. B. B. Blizanac, P. N. Ross and N. M. Marković, *J. Phys. Chem. B*, 2006, **110**, 4735-4741.
11. L. Zeng, T. S. Zhao and L. An, *J. Mater. Chem. A*, 2015, **3**, 1410-1416.
12. L. Yuan, L. Jiang, J. Liu, Z. Xia, S. Wang and G. Sun, *Electrochim. Acta*, 2014, **135**, 168-174.
13. Y. Lu, N. Zhang, L. An, X. Li and D. Xia, *J. Power Sources*, 2013, **240**, 606-611.
14. Q. Tang, L. Jiang, J. Qi, Q. Jiang, S. Wang and G. Sun, *Appl. Catal. B: Environ.*, 2011, **104**, 337-345.
15. Y. Wang, Y. Liu, X. Lu, Z. Li, H. Zhang, X. Cui, Y. Zhang, F. Shi and Y. Deng, *Electrochem. Commun.*, 2012, **20**, 171-174.
16. D. A. Slanac, W. G. Hardin, K. P. Johnston and K. J. Stevenson, *J. Am. Chem. Soc.*, 2012, **134**, 9812-9819.
17. Y. Wang, X. Lu, Y. Liu and Y. Deng, *Electrochem. Commun.*, 2013, **31**, 108-111.
18. S. Maheswari, P. Sridhar and S. Pitchumani, *Electrocatalysis*, 2012, **3**, 13-21.
19. E. J. Lim, S. M. Choi, M. H. Seo, Y. Kim, S. Lee and W. B. Kim, *Electrochem. Commun.*, 2013, **28**, 100-103.
20. Q. Wu, L. Jiang, L. Qi, L. Yuan, E. Wang and G. Sun, *Electrochim. Acta*, 2014, **123**, 167-175.
21. J. Guo, J. Zhou, D. Chu and R. Chen, *J. Phys. Chem. C*, 2013, **117**, 4006-4017.